Localized Relativistic Two-Component Methods for Ground and Excited State Calculations

Tianyuan Zhang, Joseph M. Kasper, and Xiaosong Li*

Department of Chemistry, University of Washington, Seattle, WA, 98195

E-mail: xsli@uw.edu

Abstract

Scientists are extending the computational application of relativistic methods to ever-increasing sizes of molecular systems. To this end, reduction of the computational cost of relativistic methods through modest approximations is a welcome effort. In this work, we review several localized two-component approximations and introduce a maximally localized variant. We also extend the focus of local relativistic approximations from the ground state to excited states. Benchmark calculations on both valence and core electron absorption spectra are carried out to analyze the error incurred by using the relativistic local approximations for excited state computations.

Keywords: Relativistic Electronic Structure Theory, Two-Component Theory, Local Approximation, X-ray Absorption

1 Introduction

Relativistic effects are known to be important for the description of electronic structure of heavy elements, core-electron spectroscopy, and spin-driven chemical phenomena. Relativistic electronic structure methods can be classified according to the number of complex

components in the wave function description. The most accurate approaches are based on the Dirac equation and employ a four-component wave function ansatz.[1,2] For most chemically relevant studies, exact or approximate two-component methods are usually of sufficient accuracy.

Recent developments of two-component relativistic electronic structure theories have enabled accurate description of relativistic effects in moderate-size molecular systems.[3–30] For example, relativistic two-component calculations have been used to analyze the Rashba effect in quantum confined semiconductor nanocrystals[31] and electronic structures of gold clusters.[32] In the two-component relativistic framework, the four-component equation from the Dirac equation is transformed to a related problem of half dimension to reduce the computational cost. This is possible since the four-component formalism describes both electronic and positronic degrees of freedom, yet most often it is the electronic solutions that are of interest to chemistry. In general, the four-component to two-component transformation is not a computational expensive step in relativistic calculations relative to the cost of treating electron correlation. However, because the transformation matrix is intrinsically dependent on all nuclear coordinates, analytical evaluations of molecular properties (*e.g.*, gradients, Hessians, *etc.*) become non-trivial as the response of the transformation matrix has to be computed.[32] In computing a periodic system, the transformation matrix is k-dependent and has to be evaluated for every irreducible k-point.[23] This is primarily due to the non-local spin-coupling terms because, for example, all nuclear potentials contribute to the one-electron spin-orbit coupling. To mitigate this issue, various localized four-component to two-component transformations have been proposed.[32]

Two main types of local approximations have been explored to reduce the computational cost of the two-component methods.[33–40] Here we adopt Peng and Reiher's naming conventions in Ref. 37. The first kind is the local approximation to the decoupling transformation $\mathbb{U}$ (DLU) and the second is the local approximation to the two-component Hamiltonian $\mathcal{H}^+$ (DLH). The former utilizes transformation matrices that are diagonally blocked according to

atoms or small groups of atoms in the molecular Hamiltonian. In the DLH approach, only the relativistic corrections from blocks of atoms are retained in the Hamiltonian, making it an even more localized relativistic approach.

While previous work has focused on the impact to ground state properties, in this work we compare these approximations as well as an atomically-localized two-component approach based on the ideas of diagonal local approximation to the Hamiltonian (DLH)[37] in the calculation of excited states. In particular, both valence and core-level excitations are performed in this series of calculations.

2 Methods

We use the following notation throughout the rest of this work:

- $A, B, ...$ are atomic centers.
- $\mu, \nu, ...$ are atomic orbitals.
- $i, j, ...$ are molecular orbitals.
- Calligraphic notations ($\mathcal{H}, \mathcal{U}, \cdots$) are molecular quantities in the two-component representation.
- Blackboard notations ($\mathbb{H}$, $\mathbb{U}, \cdots$) are molecular quantities in the four-component representation.

The restricted-kinetically-balanced Dirac four-component Hamiltonian in matrix form is written as[1,2]

$$\mathbb{H} = \begin{pmatrix} \mathcal{V} & \mathcal{T} \\ \mathcal{T} & \mathcal{W} - \mathcal{T} \end{pmatrix}, \tag{1}$$

where $\mathcal{V}$ and $\mathcal{T}$ are the non-relativistic potential energy and kinetic energy matrices, respectively. $\mathcal{W}$ gives rise to relativistic corrections in the Dirac Hamiltonian,

$$\mathcal{W}_{\mu\nu} = \frac{1}{4c^2} \langle \chi_\mu | \, (\boldsymbol{\sigma} \cdot \hat{\mathbf{p}}) V (\boldsymbol{\sigma} \cdot \hat{\mathbf{p}}) \, | \chi_\nu \rangle \,, \tag{2}$$

where V is the potential energy operator.

The solutions of the four-component restricted-kinetically-balanced Dirac Hamiltonian in Equation (1) are a set of bi-spinor (four-component) molecular orbitals,

$$\psi_i = \begin{pmatrix} \psi_i^L \\ \psi_i^S \end{pmatrix}, \tag{3}$$

expressed in the linear combinations of atomic orbitals (LCAO) ansatz. The large and small components (ψ_i^L and ψ_i^S) of a bi-spinor orbital are expanded in a set of basis functions centered on different nuclei ($\mathbf{R}_A$),

$$\psi_i^L = \sum_A \sum_\mu c_{i\mu}^{L,A} \chi_\mu^A (\mathbf{r} - \mathbf{R}_A), \tag{4}$$

$$\psi_i^S = \sum_A \sum_\mu c_{i\mu}^{S,A} \chi_\mu^A (\mathbf{r} - \mathbf{R}_A), \tag{5}$$

where $\chi_\mu^A(\mathbf{r} - \mathbf{R}_A)$ is a basis function centered on nucleus A. The orbital coefficients that correspond to positive and negative energy solutions can be written in a matrix form,

$$\mathbb{C} = \begin{pmatrix} \mathcal{C}^{L,+} & \mathcal{C}^{L,-} \\ \mathcal{C}^{S,+} & \mathcal{C}^{S,-} \end{pmatrix}. \tag{6}$$

In two-component methods, the electronic and positronic components of the four-component Dirac equation are decoupled by a unitary transformation $\mathbb{U}$ that block-diagonalizes the four-

component Hamiltonian:

$$\mathbb{U}^\dagger \mathbb{H} \mathbb{U} = \begin{pmatrix} \mathcal{H}^+ & \mathbf{0}_2 \\ \mathbf{0}_2 & \mathcal{H}^- \end{pmatrix}. \tag{7}$$

The exact-two-component (X2C)[13–18,35,41–48] transformation takes the form

$$\mathbb{U} = \begin{pmatrix} \mathbf{1}_2 & -\mathcal{Y}^\dagger \\ \mathcal{Y} & \mathbf{1}_2 \end{pmatrix} \begin{pmatrix} (\mathbf{1}_2 + \mathcal{Y}^\dagger \mathcal{Y})^{-1/2} & \mathbf{0}_2 \\ \mathbf{0}_2 & (\mathbf{1}_2 + \mathcal{Y}\mathcal{Y}^\dagger)^{-1/2} \end{pmatrix}, \tag{8}$$

where the matrix $\mathcal{Y}$ is calculated from the orbital coefficients as

$$\mathcal{Y} = \mathcal{C}^{S,+} (\mathcal{C}^{L,+})^{-1}. \tag{9}$$

For most chemistry problems, only the two-component Hamiltonian corresponding to electronic solutions, $\mathcal{H}^+$, needs be computed. In the one-electron X2C framework, the transformation (or "picture change") is independent of the two-electron operator. This simplification leads to a one-step procedure to construct the transformation matrix through the diagonalization of the one-electron four-component core Hamiltonian.

2.1 Local Approximation to the Two-Component Hamiltonian (DLH and ALH)

The DLH approach applies the local approximation to the construction of the Dirac Hamiltonian in the matrix form. Assume a molecular system consists of N number of atomic centers. As in Equation (1), the kinetically-balanced Dirac four-component Hamiltonian in matrix form for each atom can be written as,[1,2]

$$\mathbb{H}^A = \begin{pmatrix} \mathcal{V}^A & \mathcal{T}^A \\ \mathcal{T}^A & \mathcal{W}^A - \mathcal{T}^A \end{pmatrix}. \tag{10}$$

Given the definition of atomic block of basis functions, the atomic non-relativistic overlap matrix $\mathcal{S}^A$, kinetic energy matrix $\mathcal{T}^A$, and potential matrix $\mathcal{V}^A$, as well as the relativistic matrix $\mathcal{W}^A$ in the four-component core Hamiltonian in Equation (10) can be defined as

$$\mathcal{S}^A_{\mu\nu} = s^A_{\mu\nu} = \langle \chi^A_\mu | \chi^A_\nu \rangle, \tag{11}$$

$$\mathcal{T}^A_{\mu\nu} = t^A_{\mu\nu} = \langle \chi^A_\mu | \frac{\hat{\mathbf{p}}^2}{2} | \chi^A_\nu \rangle, \tag{12}$$

$$\mathcal{V}^A_{\mu\nu} = \sum_B v^{AB}_{\mu\nu}, \qquad v^{AB}_{\mu\nu} = -\langle \chi^A_\mu | \frac{Z_B}{|\mathbf{r} - \mathbf{R}_B|} | \chi^A_\nu \rangle, \tag{13}$$

$$\mathcal{W}^A_{\mu\nu} = \sum_B w^{AB}_{\mu\nu}, \qquad w^{AB}_{\mu\nu} = -\frac{1}{4c^2} \langle \chi^A_\mu | \frac{(\boldsymbol{\sigma} \cdot \hat{\mathbf{p}}) Z_B (\boldsymbol{\sigma} \cdot \hat{\mathbf{p}})}{|\mathbf{r} - \mathbf{R}_B|} | \chi^A_\nu \rangle, \tag{14}$$

where Z_B is the charge of nucleus B. Lowercase notations describe quantities (*e.g.*, $v^{AB}_{\mu\nu}$ and $w^{AB}_{\mu\nu}$) that only account for a single nuclear potential originated from nucleus B.

For an N-atom molecule, one can carry out N independent X2C transformations for each block using only basis functions localized on each atom of interest. This procedure results in N atomic two-component Hamiltonians $\{\mathcal{H}^A\}$. The DLH approach assumes the molecular two-component Hamiltonian has the following form,

$$\mathcal{H}^{\mathrm{DLH}} = \mathcal{V} + \mathcal{T} + \bigoplus_A \mathcal{H}^A - \bigoplus_A \mathcal{V}^A - \bigoplus_A \mathcal{T}^A \tag{15}$$

where $\mathcal{V}$ and $\mathcal{T}$ are the full molecular non-relativistic potential and kinetic energy matrices. Since the atomic diagonal blocks of $\mathcal{V}$ and $\mathcal{T}$ are also effectively included in the atomic relativistic X2C Hamiltonian $\mathcal{H}^A$, the last two terms are applied to correct for errors of double-counting.

It is clear from Equation (15) that the computational cost of four- to two-component transformation is reduced because only diagonal atomic blocks of the Hamiltonian are transformed. However, as seen from Equations (13) and (14), both potential and relativistic matrices in $\mathcal{H}^A$ still contain contributions from nuclei outside the atomic block. This suggests that the DLH Hamiltonian is still non-local, as both the atomic transformation matrix

and $\mathcal{H}^A$ depend on the coordinates of other nuclei.

In order to develop a maximally localized two-component approach, we introduce a more drastic approximation in the DLH framework. The new Hamiltonian, referred to here as the atomically localized Hamiltonian (ALH), is

$$\mathcal{H}^{\mathrm{ALH}} = \mathcal{V} + \mathcal{T} + \bigoplus_A \widetilde{\mathcal{H}}^A - \bigoplus_A v^{AA} - \bigoplus_A t^A, \tag{16}$$

where t^A and v^{AA} are defined in Equation (12) and Equation (13). In the atomic four-component Hamiltonian, $\widetilde{\mathcal{H}}^A$, $\widetilde{\mathcal{V}}^A$ and $\widetilde{\mathcal{W}}^A$ matrices no longer have contributions from other atoms in the molecule,

$$\widetilde{\mathcal{V}}^A_{\mu\nu} = v^{AA}_{\mu\nu} = -\langle \chi^A_\mu | \frac{Z_A}{|\mathbf{r} - \mathbf{R}_A|} | \chi^A_\nu \rangle, \tag{17}$$

$$\widetilde{\mathcal{W}}^A_{\mu\nu} = w^{AA}_{\mu\nu} = -\frac{1}{4c^2} \langle \chi^A_\mu | \frac{(\boldsymbol{\sigma} \cdot \hat{\mathbf{p}}) Z_A (\boldsymbol{\sigma} \cdot \hat{\mathbf{p}})}{|\mathbf{r} - \mathbf{R}_A|} | \chi^A_\nu \rangle, \tag{18}$$

making it a simple atomic, instead of atom-in-molecule, transformation. As before, the last two terms in Equation (16) account for errors of double-counting. Compared to the DLH approach, the ALH Hamiltonian ignores relativistic effects arising from off-centered potentials. As a result, the one-electron spin-orbit effect in a molecular system is only partially accounted for.

The main advantage of the ALH Hamiltonian compared to other approximations is that four- to two-component transformation is completely independent of the coordinates of other nuclei. In addition to being a low-cost relativistic two-component Hamiltonian, this makes ALH well-suited to calculations with periodic boundary conditions and also greatly simplifies the mathematical formalisms using ALH for computing relativistic molecular properties (*e.g.,* gradients, Hessian, *etc.*).

2.2 Local Approximation to the Decoupling Transformation (DLU and ALU)

A strategically different approach is to apply the local approximation to the transformation matrix. In the exact transformation, all atomic blocks are needed throughout the X2C procedure. That is, the transformation matrix $\mathbb{U}$ in Equation (8) takes the form

$$\mathbb{U} = \begin{pmatrix} U^{AA} & U^{AB} & \dots & U^{AN} \\ U^{BA} & U^{BB} & \dots & U^{BN} \\ \vdots & \vdots & \ddots & \vdots \\ U^{NA} & U^{NB} & \dots & U^{NN} \end{pmatrix} \tag{19}$$

In the DLU approximation all interatomic blocks are set to zero. That is, $\mathbb{U}$ is assumed to be of the form

$$\mathbb{U}^{\mathrm{DLU}} = \begin{pmatrix} U^{AA} & 0 & \cdots & 0 \\ 0 & U^{BB} & \cdots & 0 \\ \vdots & \vdots & \ddots & \vdots \\ 0 & 0 & \cdots & U^{NN} \end{pmatrix} \tag{20}$$

In construction of the block-diagonal atomic transformation matrix U^{AA} in DLU, all nuclear potentials in the system are included [Equations (13) and (14)]. The simplification of Equation (20) allows one to consider N small four-component localized transformation matrices instead of one with the full dimension in the diagonalization procedure. In particular, this leads to much more favorable scaling of the X2C method with respect to the number of atoms. However, we emphasize that since there is no approximation to $\mathbb{H}$, this does not lead to a block diagonal $\mathcal{H}^+$ once the transformation is applied as in Equation (7). Figure 1 graphically illustrates the main differences in the DLU and DLH approaches.

The DLU approach can be further approximated using an atomic approach similar to ALH, where the block-diagonal atomic transformation matrix U^{AA} does not include nuclear

potentials from other atoms in the system [Equations (17) and (18)], leading to the atomic local approximation to the decoupling transformation (ALU) approach.

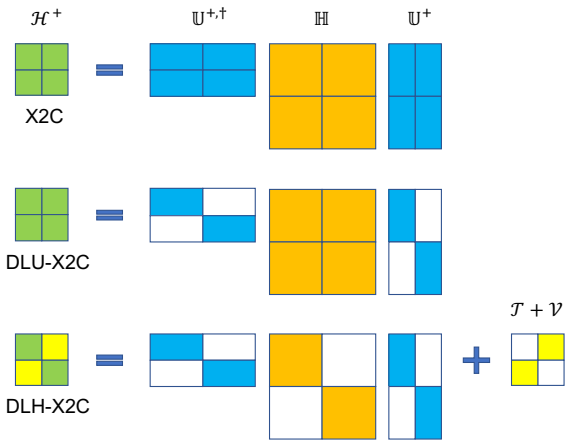

Figure 1. Graphical representation of the electronic part of the X2C transformation $\mathcal{H}^+ = \mathbb{U}^{+,\dagger}\mathbb{H}\mathbb{U}^+$ in a diatomic system, where $\mathbb{U}^+$ is the electronic part of $\mathbb{U}$. White blocks are zero submatrices in the DLU and DLH approximated approaches.

3 Result and Discussion

This work aims to benchmark various local approximations within X2C with a focus on excited state properties and potential energy surfaces. In the implementation of two-component methods, we restrict the 4c→2c transformation to the one-electron operator. Because of this approximation, an additional scaling factor for the spin-orbit coupling terms is included to account for the two electron terms in an approximate manner.[49] All approximations of X2C are implemented in the open-source Chronus Quantum package.[50] Excited state potential energy surfaces are obtained using the AO-direct formalism of relativistic TDHF[51] and TDDFT[26] in the different X2C frameworks. For brevity, we refer to the approximations to X2C, *e.g.* ALH, in the form "ALH-X2C", such as ALH-X2C-TDHF and ALH-X2C-TDDFT, compared to the full X2C approach, denoted as X2C-TDHF and X2C-TDDFT.

3.1 Pt_2 valence excited-state potential energy surfaces

To study the accuracy of the approximations in valence excited states, we use the platinum dimer (Pt_2)[52–55] as a model system as it has an open-shell ground state configuration. We compute the potential energy surfaces (PES) of the ground and first 34 excited states in the bond-length range of 2.2 to 2.7 Å with the Sapporo double-ζ[56] basis set [Sapporo(DZ)]. PES from X2C, ALU-X2C, and ALH-X2C are shown in Figure 2, and curves for the ground state and two characteristic avoided crossings are highlighted. Error statistics of all approximation schemes are listed in Table 1. Note here that both spin-orbit coupling and correlation effects are crucial in the valence electronic structure of Pt_2.[52] Since electronic correlation is not sufficiently captured in the TDHF calculation, we do not expect the simulated PES to be accurate. This comparison is merely intended to examine the accuracy of the these approximations relative to full X2C.

Table 1. Statistics of errors with respect to full X2C-TDHF results in approximated Pt_2 excited-state PES. ΔE is the error (in meV) in ground state energy, represented by non-parallelism error (NPE) and mean signed error (MSE). $\Delta\omega$ is the error (in meV) in excitation energies. Δr is the error (in pm) in curve crossing internuclear distance. Maximum error (MAX) and mean absolute error (MAE) are presented for $\Delta\omega$ and Δr. Note here there are in total 59 curve crossings in Sapporo(DZ) basis and 41 in Sapporo(DZ)+diffuse.

Approximation	ΔE/meV		$\Delta\omega$/meV		Δr/pm	
	NPE[a]	MSE	MAX	MAE	MAX	MAE
Sapporo(DZ)						
DLU	1.6	0.8	0.6	0.2	0.13	0.02
ALU	1.5	0.9	0.6	0.2	0.13	0.02
DLH	27.3	20.8	62.6	16.9	3.00	0.94
ALH	27.2	21.5	62.5	16.9	2.88	0.92
Sapporo(DZ)+diffuse						
DLU	3.8	−8.1	1.9	0.4	0.40	0.07
ALU	3.8	−8.1	1.9	0.4	0.40	0.06
DLH[b]	3926.5	−11427.7	344.6	102.5	17.81	6.70
ALH[b]	4016.0	−11567.5	419.7	129.7	29.12	10.10

[a] The non-parallelism error (NPE) is defined as the difference between maximum and minimum errors across the ground-state potential energy curve.

[b] DLH- and ALH-X2C-TDHF simulated PES in Sapporo(DZ)+diffuse do not recover all the 41 crossings in the X2C-TDHF PES. Only 29 crossings recovered and included in statistics.

In Figure 2 we do not include the results from DLU-X2C and DLH-X2C because they are not distinguishable from corresponding ALU-X2C and ALH-X2C PES, respectively. Detailed

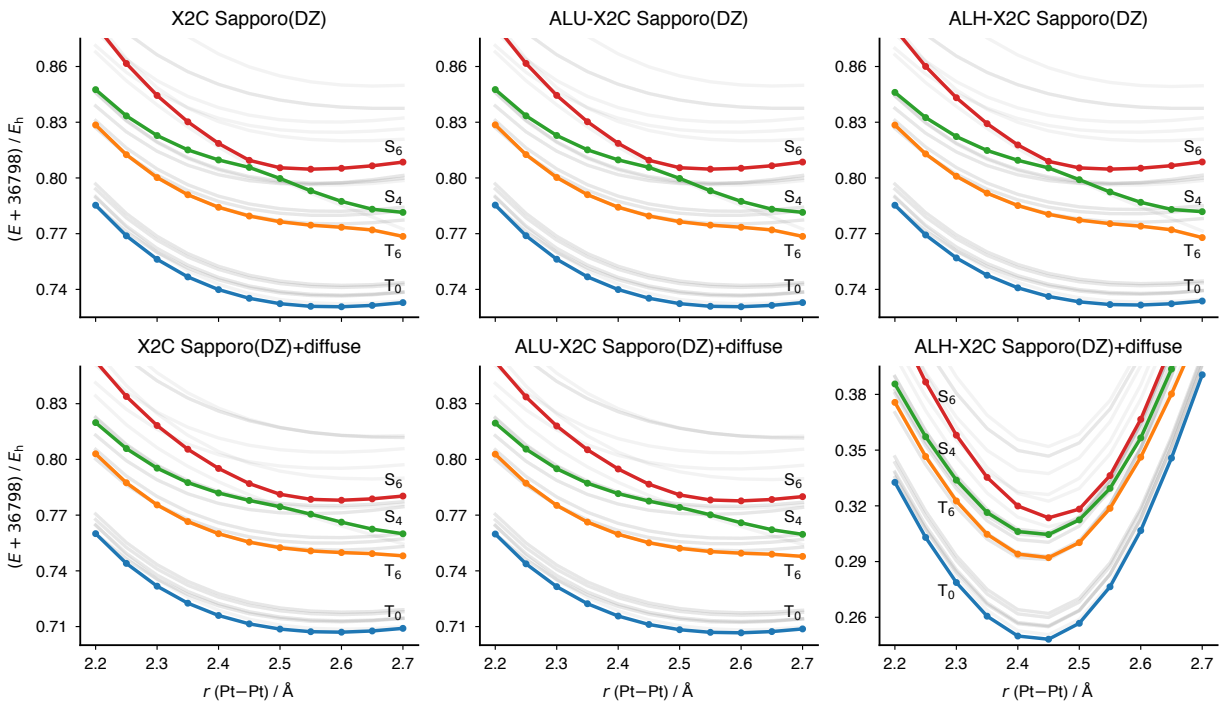

Figure 2. The first 34 excited states of Pt_2 computed using X2C-, ALU-X2C-, and ALH-X2C-TDHF methods in the Sapporo double-ζ basis set with or without diffuse functions. Most of the potential energy surfaces are shown in grey. Solid blue curves represent ground states. Orange, green, and red curves show two characteristic avoided crossings in excited states.

statistics are listed in Table 1. Overall, different atomic approximations (ALU and ALH) perform similarly compared to their corresponding diagonally localized methods (DLU and DLH). This implies that ALU and ALH are good approximations to DLU and DLH in practical applications to further reduce the computational cost of X2C based relativistic electronic structure methods. The errors in DLH and ALH are larger at shorter bond lengths and smaller at longer bond lengths. This trend is expected since the off-centered relativistic effects decrease as the distance increase, making the DLH and ALH approximations more accurate at the longer interaction distance.

In anionic molecules or systems with delocalized electronic excitations, diffuse functions are often used to improve the description of wavefunction. When PES are calculated with the Sapporo(DZ) basis set without diffuse functions, the differences between the full X2C

calculations and approximated PES in the plots are unnoticeable as shown in the upper panels in Figure 2. All 59 excited state curve crossings in the full X2C calculations are also correctly predicted by all local approximations. Table 1 reveals that errors in DLU and ALU calculations are much smaller than those using local Hamiltonian approximations (DLH and ALH). This is understandable because in DLU and ALU, the underlying Hamiltonian is still non-local and is better able to capture inter-nuclear relativistic corrections. Although the errors in DLH and ALH are $10 \sim 100$ times larger than those in DLU and ALU, they are small deviations from the full X2C calculations.

When diffuse basis functions are added in these computations, the errors in all approximation increase. The DLH- and ALH-X2C PES are qualitatively different from the full X2C calculation, while the diagonal transformation approximations (DLU and ALU) still maintain an excellent accuracy, as shown in the lower panels in Figure 2. The non-parallelism error in the ground-state potential energy curve for DLH and ALH calculations is as large as 4.0 eV, and the max and mean absolute errors in excitation energy also increase to an unacceptable range. In contrast, the errors in DLU and ALU simulations with diffuse functions are only about 3 times greater than those without diffuse functions and still in excellent agreement with the full X2C results.

The error in local Hamiltonian approximations (DLH and ALH) primarily arises from neglect of the relativistic transformation to the off-diagonal matrix elements $\left\langle \chi^A \right| \hat{h} \left| \chi^B \right\rangle$ where $A \neq B$. When diffuse functions are introduced into the system, their significant overlaps with valence electron atomic orbitals in nonorthogonal atomic basis lead to a non-negligible off-diagonal contribution. Ignoring these large terms in the transformation will result in a significant change of the electronic characteristics of valence electrons. As such, local Hamiltonian approximations (DLH and ALH) with diffuse functions are not good methods for describe relativistic effects in ground state and low-energy valence excited state.

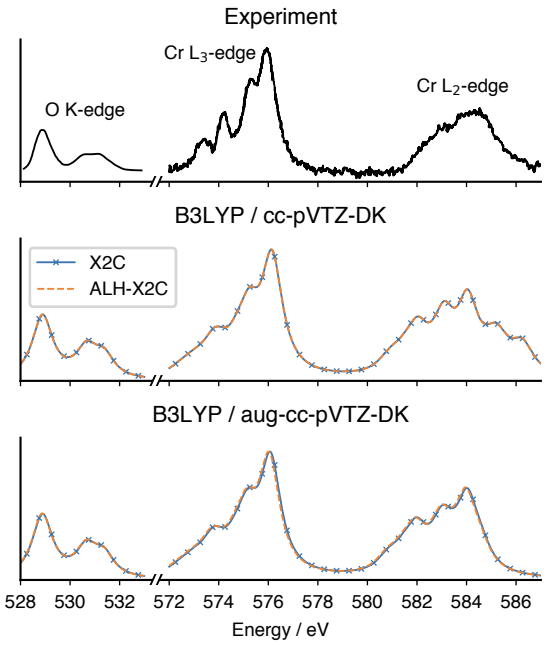

Figure 3. The upper panel is the experimental oxygen K-edge and chromium $L_{2,3}$-edge spectra.[57] The middle and lower panel shows TDDFT simulated spectra computed in cc-pVTZ-DK and aug-cc-pVTZ-DK basis sets with B3LYP functional. Simulated spectra are shifted 12.5 and 6.2 eV for O K-edge and Cr $L_{2,3}$-edge, respectively, to match experimental spectra. A Lorentzian broadening parameter of 0.5 eV was used to plot the simulated spectra. The geometry of CrO_2Cl_2 is from Ref. 26.

3.2 Transition metal complex $L_{2,3}$-edge X-ray absorption spectra

To investigate the accuracy of local approximations in simulating core electron excitation, we compute the chromium $L_{2,3}$-edge X-ray absorption spectra of the CrO_2Cl_2 molecule with linear-response non-collinear time-dependent density functional theory (TDDFT)[46,47,58] and B3LYP exchange-correlation functional.[59–61] The excitation oscillator strengths in this work are computed with dipole operator directly applied in the X2C transformed basis without considering the picture-change effect.[43,62] Table 2 lists error analyses of Cr L-edge calculations using different local X2C approximations. As is standard practice in computations involving core electron excitations, a uniform shift is applied to the full X2C simulated X-ray spectra so that the main L_3 peak matches the experiment. The same amount of shift is applied to all local approximations, and statistical analyses (MAX and MAE) are carried out. We

also define the shifted mean absolute error (S-MAE) to analyze excitation energies when the approximated spectra are independently shifted instead of using the shift amount for the full X2C calculation.

As already reported in Ref. 26, with appropriate shifts, the X2C-TDDFT simulated spectra agree well with the experimental measurement. We observe a similar trend and behavior for all local approximations compared to those for the valence excitations discussed in the previous section. In most cases, the differences between local approximations and the full X2C calculations are on the order of a few meV for excitation energy MAE and less than 1% for oscillator strength MAE. Comparably, DLU- and ALU- approximated results are more accurate than those with DLH and ALH approximations. This is especially true for ground-state absolute energies and in the presence of diffuse basis functions. Although the error in ground state energy can be significant, the excitation energies computed using local approximation are all in excellent agreement with the full X2C calculations. This is because the relativistic effect in core-electron excitation is mostly local. As such, local approximations are well-suited for computing X-ray absorption spectroscopies. Using diffuse functions seems to introduce a relatively larger error but not as significant as that for valence excitations. If the spectra computed using local approximations are shifted independently so that their respective main L_3 peaks are aligned with experiments, the shifted mean absolute error (S-MAE) is reduced to less than 1 meV. This means the error introduced by local approximations is mostly manifested as a constant energy shift.

In Figure 3 we overlap the most drastic approximation (ALH-X2C-TDDFT) and X2C-TDDFT simulated X-ray absorption spectra in cc-pVTZ-DK and aug-cc-pVTZ-DK[63–65] basis sets. In cc-pVTZ-DK basis set, the near-perfect overlap between X2C-TDDFT and ALH-X2C-TDDFT results in Figure 3 demonstrates that the local approximations do not introduce noticeable error on both excitation energies and oscillator strengths. With diffuse functions in the aug-cc-pVTZ-DK basis set, the ALH approximated spectra still recovers the shape of the reference X2C-TDDFT ones, but the $L_{2,3}$-edge spectra appears to be slightly red shifted.

According to the statistics in Table 2, the errors in the aug-cc-pVTZ-DK ALH-X2C-TDDFT $L_{2,3}$-edge spectra are up to 54 meV, which mostly arises from the spectral shift constant as discussed above.

To demonstrate the accuracy of simulating XAS with the most drastic approximation (ALH-X2C-TDDFT method) in different molecular systems, in Table 3 we list the statistical error analyses between ALH-X2C and full X2C simulations of $SiCl_4$ and four transition-metal-complex $L_{2,3}$-edge spectra. Additionally, these calculations compare two different density functional methods (B3LYP[59–61] and PBE0[66–68]) and two basis sets [6-311G(d)[69–74] and Sapporo double-ζ[75]]. Note that Pd does not have an associated 6-311G(d) basis set. We also note here that only peaks with oscillator strengths greater than 0.01 (0.004 for $PdCl_2$) are included in our statistics to avoid large relative numerical error.

As seen in Table 3, the difference in errors between the B3LYP and PBE0 functionals are much less than the difference between the 6-311G(d) and Sapporo(DZ) basis sets. This is because the approximations are applied to the one-electron Hamiltonian but have no influence on the electron repulsion integrals. Consequently, the approximation does not contribute significantly to exchange and correlation effects, and the errors are essentially functional independent.

For all systems considered here, the ALH approximation has a maximum error up to 3% and mean absolute error less than 1% in oscillator strength. For first-row transition metal complexes (Ti, V, and Cr), according to the statistics in Table 3, the ALH approximation has a maximum error of 1$\sim$4 meV in excitation energy, which is smaller than the errors in ground state energy. The errors in both ground state and excitation energies for Si and Pd complexes can be as large as 18 meV, likely due to a strong coupling between Si/Pd with Cl ligands. Considering the large L-edge excitation energies, however, this error is still relatively small.

In contrast to the poor performance of local Hamiltonian approximations (DLH and ALH) with diffuse functions for describing valence excited states in the Pt_2 case, these

approximated X2C approaches seem to work well for core-electron excitations even in the presence of diffuse functions. While diffuse functions have large overlap with valence atomic orbitals, their overlaps with the highly-localized core electron orbitals remain small and do not significantly modify the electronic structures of core electrons. As a result, the computed spectra are in excellent agreement with the full X2C results.

4 Conclusion

In this work, we reviewed and studied localized approximations to the two-component relativistic Hamiltonian, including atomic-localized variants. In performance benchmarks, the ALH- and ALU-X2C methods reproduce well the results of the DLH- and DLU-X2C simulations with negligible loss of accuracy.

All approximated results, including those from the maximally localized ALH-X2C approximation, are almost indistinguishable from the X2C reference for systems that do not include diffuse basis functions. Including diffuse basis functions in computations introduces significant error in the ground-state absolute energies and low-lying valence excited states predicted by DLH and ALH approximations. This is because the strong overlap between the diffuse functions and valence electron orbitals. Ignoring these contributions in local Hamiltonian approximations (DLH and ALH) will significantly change the underlying electronic structures.

However, due to the small overlap between diffuse functions and core-electron orbitals, all local approximations, including, DLU, DLH, ALU, and ALH, are well-suited for computing core-electron excited states. All calculations exhibit excellent agreement, in both the excitation energy and oscillator strength, with the full X2C result in computing K- and L-edge X-ray absorption spectra.

Acknowledgement

The development of two-component relativistic electronic structure method is funded by the US Department of Energy (DE-SC0006863). The development of non-perturbative spectroscopic methods is supported by the National Science Foundation (CHE-1856210). The development of the Chronus Quantum open source software package is supported by the National Science Foundation (OAC-1663636). T. Z. thanks Shichao Sun, Torin Stetina, and Hongbin Liu for valuable discussion.

References

(1) Dyall, K. G.; Fægri, Jr., K. *Introduction to Relativistic Quantum Chemistry*; Oxford University Press, 2007.

(2) Reiher, M.; Wolf, A. *Relativistic Quantum Chemistry*, 2nd ed.; Wiley-VCH, 2015.

(3) Hess, B. A. Relativistic Electronic-Structure Calculations Employing a Two-Component No-Pair Formalism with External-Field Projection Operators. *Phys. Rev. A* **1986**, *33*, 3742–3748.

(4) Jansen, G.; Hess, B. A. Revision of the Douglas-Kroll transformation. *Phys. Rev. A* **1989**, *39*, 6016–6017.

(5) Filatov, M.; Cremer, D. Representation of the exact relativistic electronic Hamiltonian within the regular approximation. *J. Chem. Phys.* **2003**, *119*, 11526–11540.

(6) Filatov, M.; Cremer, D. Connection between the regular approximation and the normalized elimination of the small component in relativistic quantum theory. *J. Chem. Phys.* **2005**, *122*, 064104.

(7) Kutzelnigg, W.; Liu, W. Quasirelativistic theory I. Theory in terms of a quasirelativistic operator. *Mol. Phys.* **2006**, *104*, 2225–2240.

(8) Reiher, M. Douglas–Kroll–Hess Theory: a relativistic electrons-only theory for chemistry. *Theor. Chem. Acc.* **2006**, *116*, 241–252.

(9) Filatov, M.; Dyall, K. G. On convergence of the normalized elimination of the small component (NESC) method. *Theor. Chem. Acc.* **2006**, *117*, 333–338.

(10) Liu, W.; Kutzelnigg, W. Quasirelativistic theory. II. Theory at matrix level. *J. Chem. Phys.* **2007**, *126*, 114107.

(11) Autschbach, J. Density functional theory applied to calculating optical and spectroscopic properties of metal complexes: NMR and optical activity. *Coordin. Chem. Rev.* **2007**, *251*, 1796–1821.

(12) Sikkema, J.; Visscher, L.; Saue, T.; Iliaš, M. The molecular mean-field approach for correlated relativistic calculations. *J. Chem. Phys.* **2009**, *131*, 124116.

(13) Liu, W.; Peng, D. Infinite-Order Quasirelativistic Density Functional Method Based on the Exact Matrix Quasirelativistic Theory. *J. Chem. Phys.* **2006**, *125*, 044102.

(14) Liu, W.; Peng, D. Exact Two-component Hamiltonians Revisited. *J. Chem. Phys.* **2009**, *131*, 031104.

(15) Kutzlenigg, W.; Liu, W. Quasirelativistic Theory Equivalent to Fully Relativistic Theory. *J. Chem. Phys.* **2005**, *123*, 241102.

(16) Liu, W. Ideas of Relativistic Quantum Chemistry. *Mol. Phys.* **2010**, *108*, 1679–1706.

(17) Ilias, M.; Saue, T. An Infinite-Order Relativistic Hamiltonian by a Simple One-Step Transformation. *J. Chem. Phys.* **2007**, *126*, 064102.

(18) Saue, T. Relativistic Hamiltonians for Chemistry: A Primer. *ChemPhysChem* **2011**, *12*, 3077–3094.

(19) Nakajima, T.; Hirao, K. The Douglas–Kroll–Hess Approach. *Chem. Rev.* **2011**, *112*, 385–402.

(20) Reiher, M. Relativistic Douglas-Kroll-Hess theory. *WIREs Comput. Mol. Sci.* **2011**, *2*, 139–149.

(21) Peng, D.; Reiher, M. Exact decoupling of the relativistic Fock operator. *Theor. Chem. Acc.* **2012**, *131*, 2037–20.

(22) Autschbach, J.; Peng, D.; Reiher, M. Two-Component Relativistic Calculations of Electric-Field Gradients Using Exact Decoupling Methods: Spin–orbit and Picture-Change Effects. *J. Chem. Theory Comput.* **2012**, *8*, 4239–4248.

(23) Zhao, R.; Zhang, Y.; Xiao, Y.; Liu, W. Exact two-component relativistic energy band theory and application. *J. Chem. Phys.* **2016**, *144*, 044105.

(24) Kasper, J. M.; Lestrange, P. J.; Stetina, T. F.; Li, X. Modeling $L_{2,3}$-Edge X-ray Absorption Spectroscopy with Real-Time Exact Two-Component Relativistic Time-Dependent Density Functional Theory. *J. Chem. Theory Comput.* **2018**, *14*, 1998–2006.

(25) Franzke, Y. J.; Middendorf, N.; Weigend, F. Efficient implementation of one- and two-component analytical energy gradients in exact two-component theory. *J. Chem. Phys.* **2018**, *148*, 104110.

(26) Stetina, T. F.; Kasper, J. M.; Li, X. Modeling $L_{2,3}$-Edge X-ray Absorption Spectroscopy with Linear Response Exact Two-Component Relativistic Time-Dependent Density Functional Theory. *J. Chem. Phys.* **2019**, *150*, 234103.

(27) Kadek, M.; Repisky, M.; Ruud, K. All-electron fully relativistic Kohn-Sham theory for solids based on the Dirac-Coulomb Hamiltonian and Gaussian-type functions. *Phys. Rev. B* **2019**, *99*, 205103.

(28) Koulias, L. N.; Williams-Young, D. B.; Nascimento, D. R.; DePrince, A. E.; Li, X. Relativistic Time-Dependent Equation-of-Motion Coupled-Cluster. *J. Chem. Theory Comput.* **2019**, *15*, 6617–6624.

(29) Jenkins, A. J.; Liu, H.; Kasper, J. M.; Frisch, M. J.; Li, X. Variational Relativistic Complete Active Space Self-Consistent Field Method. *J. Chem. Theory Comput.* **2019**, *15*, 2974–2982.

(30) Hu, H.; Jenkins, A. J.; Liu, H.; Kasper, J. M.; Frisch, M. J.; Li, X. Relativistic Two-Component Multireference Configuration Interaction Method with Tunable Correlation Space. *J. Chem. Theory Comput.* **2020**, *16*, 2975–2984.

(31) Kasper, J. M.; Gamelin, D. R.; Li, X. Theoretical Investigation of Quantum Confinement on the Rashba Effect in ZnO Semiconductor Nanocrystals. *J. Chem. Phys.* **2020**, *152*, 014308.

(32) Zou, W.; Guo, G.; Suo, B.; Liu, W. Analytic Energy Gradients and Hessians of Exact Two-Component Relativistic Methods: Efficient Implementation and Extensive Applications. *J. Chem. Theory Comput.* **2020**, *16*, 1541–1554.

(33) Gagliardi, L.; Handy, N. C.; Ioannou, A. G.; Skylaris, C.-K.; Spencer, S.; Willetts, A.; Simper, A. M. A two-centre implementation of the Douglas–Kroll transformation in relativistic calculations. *Chem. Phys. Lett.* **1998**, *283*, 187–193.

(34) Dyall, K. G.; Enevoldsen, T. Interfacing relativistic and nonrelativistic methods. III. Atomic 4-spinor expansions and integral approximations. *J. Chem. Phys.* **1999**, *111*, 10000–10007.

(35) Peng, D.; Liu, W.; Xiao, Y.; Cheng, L. Making Four- and Two-Component Relativistic Density Functional Methods Fully Equivalent Based on the Idea of From Atoms to Molecule. *J. Chem. Phys.* **2007**, *127*, 104106.

(36) Matveev, A. V.; Rösch, N. Atomic approximation to the projection on electronic states in the Douglas-Kroll-Hess approach to the relativistic Kohn-Sham method. *J. Chem. Phys.* **2008**, *128*, 244102.

(37) Peng, D.; Reiher, M. Local relativistic exact decoupling. *J. Chem. Phys.* **2012**, *136*, 244108.

(38) Seino, J.; Nakai, H. Local unitary transformation method for large-scale two-component relativistic calculations: Case for a one-electron Dirac Hamiltonian. *J. Chem. Phys.* **2012**, *136*, 244102.

(39) Seino, J.; Nakai, H. Local unitary transformation method for large-scale two-component relativistic calculations. II. Extension to two-electron Coulomb interaction. *J. Chem. Phys.* **2012**, *137*, 144101.

(40) Laikov, D. N. Additive atomic approximation for relativistic effects: A two-component Hamiltonian for molecular electronic structure calculations. *J. Chem. Phys.* **2019**, *150*, 061103.

(41) Li, Z.; Xiao, Y.; Liu, W. On the Spin Separation of Algebraic Two-Component Relativistic Hamiltonians. *J. Chem. Phys.* **2012**, *137*, 154114.

(42) Peng, D.; Middendorf, N.; Weigend, F.; Reiher, M. An Efficient Implementation of Two-Component Relativistic Exact-Decoupling Methods for Large Molecules. *J. Chem. Phys.* **2013**, *138*, 184105.

(43) Egidi, F.; Goings, J. J.; Frisch, M. J.; Li, X. Direct Atomic-Orbital-Based Relativistic Two-Component Linear Response Method for Calculating Excited-State Fine Structures. *J. Chem. Theory Comput.* **2016**, *12*, 3711–3718.

(44) Goings, J. J.; Kasper, J. M.; Egidi, F.; Sun, S.; Li, X. Real Time Propagation of the Exact Two Component Time-Dependent Density Functional Theory. *J. Chem. Phys.* **2016**, *145*, 104107.

(45) Konecny, L.; Kadek, M.; Komorovsky, S.; Malkina, O. L.; Ruud, K.; Repisky, M. Acceleration of Relativistic Electron Dynamics by Means of X2C Transformation: Application to the Calculation of Nonlinear Optical Properties. *J. Chem. Theory Comput.* **2016**, *12*, 5823–5833.

(46) Egidi, F.; Sun, S.; Goings, J. J.; Scalmani, G.; Frisch, M. J.; Li, X. Two-Component Non-Collinear Time-Dependent Spin Density Functional Theory for Excited State Calculations. *J. Chem. Theory Comput.* **2017**, *13*, 2591–2603.

(47) Petrone, A.; Williams-Young, D. B.; Sun, S.; Stetina, T. F.; Li, X. An Efficient Implementation of Two-Component Relativistic Density Functional Theory with Torque-Free Auxiliary Variables. *Euro. Phys. J. B* **2018**, *91*, 169.

(48) Liu, W.; Xiao, Y. Relativistic Time-dependent Density Functional Theories. *Chem. Soc. Rev.* **2018**, *47*, 4481–4509.

(49) Boettger, J. C. Approximate Two-Electron Spin-Orbit Coupling Term For Density-Functional-Theory DFT Calculations Using The Douglas-Kroll-Hess Transformation. *Phys. Rev. B* **2000**, *62*, 7809–7815.

(50) Williams-Young, D. B.; Petrone, A.; Sun, S.; Stetina, T. F.; Lestrange, P.; Hoyer, C. E.; Nascimento, D. R.; Koulias, L.; Wildman, A.; Kasper, J.; Goings, J. J.; Ding, F.; DePrince III, A. E.; Valeev, E. F.; Li, X. The Chronus Quantum (ChronusQ) Software Package. *WIREs Comput. Mol. Sci.* **2019**, e1436.

(51) Goings, J. J.; Ding, F.; Davidson, E. R.; Li, X. Approximate Singly Excited States from a Two-Component Hartree Fock Reference. *J. Chem. Phys.* **2015**, *143*, 144106.

(52) Balasubramanian, K. Electronic states of Pt_2. *J. Chem. Phys.* **1987**, *87*, 6573–6578.

(53) Ho, J.; Polak, M. L.; Ervin, K. M.; Lineberger, W. C. Photoelectron spectroscopy of nickel group dimers: Ni_2^-, Pd_2^-, and Pt_2^-. *J. Chem. Phys.* **1993**, *99*, 8542–8551.

(54) Strandberg, T. O.; Canali, C. M.; MacDonald, A. H. Transition-metal dimers and physical limits on magnetic anisotropy. *Nat. Mater.* **2007**, *6*, 648–651.

(55) Błoński, P.; Dennler, S.; Hafner, J. Strong spin–orbit effects in small Pt clusters: Geometric structure, magnetic isomers and anisotropy. *J. Chem. Phys.* **2011**, *134*, 034107.

(56) Noro, T.; Sekiya, M.; Koga, T. Sapporo-(DKH3)-nZP (n = D, T, Q) sets for the sixth period s-, d-, and p-block atoms. *Theor. Chem. Acc.* **2013**, *132*, 1124.

(57) Fronzoni, G.; Stener, M.; Decleva, P.; de Simone, M.; Coreno, M.; Franceschi, P.; Furlani, C.; Prince, K. C. X-ray Absorption Spectroscopy of $VOCl_3$, CrO_2Cl_2, and MnO_3Cl: An Experimental and Theoretical Study. *J. Phys. Chem. A* **2009**, *113*, 2914–2925.

(58) Goings, J. J.; Egidi, F.; Li, X. Current Development of Non-collinear Electronic Structure Theory. *Int. J. Quant. Chem.* **2018**, *118*, e25398.

(59) Becke, Axel D, Density-functional thermochemistry. III. The role of exact exchange. *J. Chem. Phys.* **1993**, *98*, 5648–5652.

(60) Lee, Chengteh,; Yang, Weitao,; Parr, Robert G, Development of the Colle-Salvetti correlation-energy formula into a functional of the electron density. *Phys. Rev., B Condens. Matter* **1988**, *37*, 785–789.

(61) Miehlich, Burkhard,; Savin, Andreas,; Stoll, Hermann,; Preuss, Heinzwerner, Results obtained with the correlation energy density functionals of becke and Lee, Yang and Parr. *Chem. Phys. Lett.* **1989**, *157*, 200–206.

(62) Wolf, Alexander,; Reiher, Markus, Exact decoupling of the Dirac Hamiltonian. III. Molecular properties. *J. Chem. Phys.* **2006**, *124*, 064102.

(63) Dunning Jr, T. H. Gaussian basis sets for use in correlated molecular calculations. I. The atoms boron through neon and hydrogen. *J. Chem. Phys.* **1989**, *90*, 1007–1018.

(64) Woon, D. E.; Dunning Jr, T. H. Gaussian basis sets for use in correlated molecular calculations. III. The atoms aluminum through argon. *J. Chem. Phys.* **1993**, *98*, 1358–1371.

(65) Balabanov, N. B.; Peterson, K. A. Systematically convergent basis sets for transition metals. I. All-electron correlation consistent basis sets for the $3d$ elements Sc–Zn. *J. Chem. Phys.* **2005**, *123*, 064107–064116.

(66) Perdew, John P,; Burke, Kieron,; Ernzerhof, Matthias, Generalized Gradient Approximation Made Simple. *Phys. Rev. Lett.* **1996**, *77*, 3865–3868.

(67) Perdew, J. P.; Burke, K.; Ernzerhof, M. Errata: Generalized Gradient Approximation Made Simple [Phys. Rev. Lett. 77, 3865 (1996)]. *Phys. Rev. Lett.* **1997**, *78*, 1396–1396.

(68) Adamo, Carlo,; Barone, Vincenzo, Toward reliable density functional methods without adjustable parameters: The PBE0 model. *J. Chem. Phys.* **1999**, *110*, 6158–6170.

(69) Krishnan, R,; Binkley, J S,; Seeger, R,; Pople, J A, Self-consistent molecular orbital methods. XX. A basis set for correlated wave functions. *J. Chem. Phys.* **1980**, *72*, 650–654.

(70) McLean, A D,; Chandler, G S, Contracted Gaussian basis sets for molecular calculations. I. Second row atoms, Z=11–18. *J. Chem. Phys.* **1980**, *72*, 5639–5648.

(71) Francl, Michelle M,; Pietro, William J,; Hehre, Warren J,; Binkley, J Stephen,; Gordon, Mark S,; DeFrees, Douglas J,; Pople, John A, Self-consistent molecular orbital methods. XXIII. A polarization-type basis set for second-row elements. *J. Chem. Phys.* **1982**, *77*, 3654–3665.

(72) Wachters, A J H, Gaussian Basis Set for Molecular Wavefunctions Containing Third-Row Atoms. *J. Chem. Phys.* **1970**, *52*, 1033–1036.

(73) Hay, P Jeffrey, Gaussian basis sets for molecular calculations. The representation of $3d$ orbitals in transition-metal atoms. *J. Chem. Phys.* **1977**, *66*, 4377–4384.

(74) Raghavachari, Krishnan,; Trucks, Gary W, Highly correlated systems. Excitation energies of first row transition metals Sc–Cu. *J. Chem. Phys.* **1989**, *91*, 1062–1065.

(75) Noro, T.; Sekiya, M.; Koga, T. Segmented contracted basis sets for atoms H through Xe: Sapporo-(DK)-nZP sets (n = D, T, Q). *Theor. Chem. Acc.* **2012**, *131*, 25.

Table 2. Error analyses of simulated Cr L-edge X-ray absorption spectra of CrO_2Cl_2 using different local approximations with non-collinear B3LYP and various basis sets, compared to those computed using full X2C-TDDFT. All N_{peak} peaks with oscillator strengths greater than 0.01 are included in the statistics. ΔE is the absolute error (in meV) in ground state energy. $\Delta\omega$ is the error (in meV) in excitation energies. $\Delta f\%$ is the percent error in oscillator strength. Maximum error (MAX) and mean absolute error (MAE) are presented for ΔE and $\Delta f\%$. In addition, shifted MAE (S-MAE) is presented for $\Delta\omega$. The molecule geometry is available in Ref. 26.

Approximation	ΔE/meV	N_{peak}	$\Delta\omega$/meV			$\Delta f\%$	
			MAX	MAE	S-MAE	MAX	MAE
6-311G(d)							
DLU	6.52	13	0.94	0.23	0.20	1.57	0.21
ALU	6.52	13	0.13	0.05	0.05	1.57	0.21
DLH	12.63	13	1.53	0.57	0.47	1.92	0.34
ALH	11.74	13	1.56	0.57	0.47	0.61	0.14
6-311+G(d)							
DLU	4.76	12	0.07	0.04	0.03	0.00	0.00
ALU	4.76	12	0.07	0.04	0.03	0.00	0.00
DLH	−75.42	12	3.41	2.92	0.20	4.85	0.67
ALH	−76.67	12	3.49	2.91	0.18	6.67	0.86
Sapporo(DZ)							
DLU	0.53	13	0.21	0.11	0.05	0.13	0.01
ALU	0.53	13	0.21	0.11	0.05	0.13	0.01
DLH	6.57	13	3.99	2.68	0.27	0.13	0.02
ALH	6.28	13	3.96	2.73	0.26	0.13	0.02
Sapporo(DZ)+diffuse							
DLU	0.45	13	0.41	0.16	0.06	0.65	0.11
ALU	0.45	13	0.41	0.16	0.05	0.65	0.11
DLH	−227.41	13	1.27	0.67	0.35	1.20	0.25
ALH	−228.76	13	1.30	0.68	0.32	1.81	0.32
cc-pVDZ-DK							
DLU	2.06	13	0.10	0.04	0.03	0.10	0.01
ALU	2.07	13	0.09	0.03	0.02	0.10	0.01
DLH	−0.28	13	3.23	2.60	0.29	0.68	0.24
ALH	−0.70	13	3.09	2.58	0.28	0.68	0.22
aug-cc-pVDZ-DK							
DLU	0.37	12	0.69	0.58	0.03	0.48	0.07
ALU	0.37	12	0.69	0.58	0.03	0.48	0.07
DLH	−572.14	12	53.93	52.82	0.65	2.11	0.35
ALH	−575.41	12	54.47	53.52	0.52	1.22	0.30

Table 3. Error analyses of the ALH-X2C simulated L-edge X-ray absorption spectra of five molecules with different functionals and basis sets, compared to those computed using full X2C-TDDFT. All N_{peak} peaks with oscillator strengths greater than 0.01 (0.004 for $PdCl_2$) are included in the statistics. ΔE is the absolute error (in meV) in ground state energy. $\Delta\omega$ is the error (in meV) in excitation energies. $\Delta f\%$ is the percent error in oscillator strength. Maximum error (MAX) and mean absolute error (MAE) are presented for $\Delta\omega$ and $\Delta f\%$. In addition, shifted MAE (S-MAE) is presented for $\Delta\omega$. Geometries and spectra plots are available in Ref. 26.

Basis	Functional	ΔE/meV	N_{peak}	$\Delta\omega$/meV			$\Delta f\%$	
				MAX	MAE	S-MAE	MAX	MAE
$SiCl_4$ Si $L_{2,3}$-edge								
6-311G(d)	B3LYP	2.73	8	18.48	9.64	4.72	2.56	0.65
6-311G(d)	PBE0	3.65	9	17.40	9.28	4.45	2.17	0.69
sapporo(dz)	B3LYP	−17.60	8	14.55	6.62	4.77	0.60	0.24
sapporo(dz)	PBE0	−16.29	8	13.73	6.53	4.81	0.85	0.27
$TiCl_4$ Ti $L_{2,3}$-edge								
6-311G(d)	B3LYP	3.12	5	0.94	0.74	0.14	2.38	0.61
6-311G(d)	PBE0	2.88	4	1.09	0.72	0.28	0.00	0.00
sapporo(dz)	B3LYP	−8.94	4	2.81	2.51	0.23	0.00	0.00
sapporo(dz)	PBE0	−7.89	4	2.75	2.50	0.22	0.09	0.02
$VOCl_3$ V $L_{2,3}$-edge								
6-311G(d)	B3LYP	8.12	10	0.79	0.31	0.22	0.32	0.03
6-311G(d)	PBE0	7.88	10	0.86	0.32	0.25	0.17	0.03
sapporo(dz)	B3LYP	−1.22	10	1.20	0.91	0.16	0.27	0.06
sapporo(dz)	PBE0	−0.52	10	1.15	0.90	0.18	0.48	0.10
CrO_2Cl_2 Cr $L_{2,3}$-edge								
6-311G(d)	B3LYP	11.74	13	1.56	0.57	0.47	0.61	0.14
6-311G(d)	PBE0	11.52	15	0.98	0.46	0.45	0.85	0.10
sapporo(dz)	B3LYP	6.28	13	3.96	2.73	0.26	0.13	0.02
sapporo(dz)	PBE0	6.27	13	3.71	2.64	0.29	0.45	0.10
$PdCl_2$ Pd $L_{2,3}$-edge								
sapporo(dz)	B3LYP	−14.34	3	12.51	7.39	3.41	0.00	0.00
sapporo(dz)	PBE0	−13.46	3	5.89	4.79	4.42	1.69	0.56